Metamaterials for Space Applications

Design of invisibility cloaks for reduced observability of objects

Final Report

Authors: F. Bilotti, S. Tricarico, L. Vegni
Affiliation: University Roma Tre

ESA Researcher(s): Jose M. Llorens and Luzi Bergamin

Date: 20.7.2008

Contacts:

Filiberto Bilotti
Tel: +39.06.57337096
Fax: +39.06.57337026
e-mail: bilotti@uniroma3.it

Leopold Summerer
Tel: +31(0)715655174
Fax: +31(0)715658018
e-mail: act@esa.int

Available on the ACT website
http://www.esa.int/act

Ariadna ID: 07/7001b
Study Duration: 4 months
Contract Number: 21263/07/NL/CB

Contents

Abstract

We firstly present the design of an electromagnetic cloaking device working for both TE and TM polarizations at microwaves. The theoretical approach to cloaking here used is inspired to the one presented by Alù and Engheta [1]. The case of TE polarization is firstly considered and, then, an actual inclusion-based cloak for the TE polarization is also designed. In such a case, the cloak is made of a Mu-Near-Zero (MNZ) metamaterial, as the dual counterpart of the Epsilon-Near-Zero (ENZ) material that can be used for purely dielectric objects. The operation and the robustness of the cloaking device for the TE polarization are deeply investigated through a complete set of full-wave numerical simulations. Then, the design and an application of a cloak operating for both the TE and TM polarizations employing both magnetic inclusions and the parallel plate medium already used by Silveirinha et al. [2] are presented. We extend then the previous results to the design of cylindrical and spherical electromagnetic cloaks working at visible frequencies. The cloak design is based on the employment of layered structures consisting of alternating plasmonic and non-plasmonic materials and exhibiting the collective behavior of an effective epsilon-near-zero material at optical frequencies. Two alternative layouts are proposed and both magnetic and non-magnetic objects are considered. Then, the design of spherical cloaks is also presented. The effect of the losses is also considered. We finally study the effect of a cloaking device on the radiation pressure exerted on cylindrical and spherical particles.

Objectives of the study

Recently, numerous works have suggested the idea that is possible to create a cloak of invisibility in a given frequency band. Achieving transparency or low scattering by employing a proper engineered cover is a common issue in literature, however the solutions proposed by standard techniques, for example absorbers or anti-reflection coatings, have strict limitations with reference to the shape and material of the cloaked object. In order to overcome such restrictions, various authors have suggested applying the unusual properties of Metamaterials, artificial materials synthesized by inserting several metallic or dielectric inclusions into a host material. With reference to this type of materials, the possibility of having atypical values of permittivity and/or permeability can help designing new artificial structured covers which are able to dramatically decrease the scattering of the cloaked object. Different approaches have been developed by different research groups worldwide [1-13] for designing such covers, and even if a proper comparison between all these approaches has not be developed so far, we may say that each of them, though based on different physics, clearly shows advantages, but also undoubted limitations. For instance, the theoretical approach based on the coordinate transformation [5]-[11], which is very elegant from the mathematical and physical point of views, works quite well even for large objects, and is independent of the object to cloak, may find some problems at the fabrication stage, due to the employment of the reduced parameters and to the inhomogeneity of the cloak material. Nevertheless, some experiments have been already conducted with a certain degree of success [11]. As for any metamaterial design, anyway, losses play an important role, as these experiments clearly reveal. Apart from these difficulties, even from the fundamental point of view there are some problems, especially if we are interested in cloaking devices working not only at a single frequency. In the coordinate transformation approach, in fact, the paths of the electromagnetic field circumventing the object are covered with a phase velocity which is greater than the speed of light. Anyway, when a pulsed electromagnetic field impinges on the object covered with the cloak, since the group velocity does not excides the speed of light, the resulting cloak cannot have the desired functionality over a broad range of frequencies, even if we are able to realize broadband metamaterials. On the other hand, as it is well known from the microwave circuit theory, losses are inherently related to any impedance transformation, even in the case of continuous transformation. For

this reason, cloaks based on this approach must be quite large in order to have a very smooth variation of the parameters and reduce the losses as much as possible. Also the approach based on plasmonic materials proposed in [1,2] is characterized by advantages and disadvantages. One limitation is that this approach is, to some extent, object-dependent. Though some new results have been presented recently, showing that the shape of the object can be changed a little, while keeping the operation of the cloak [3], the object cannot be anyway changed in a substantial way. Another potential drawback of this approach resides in the dimensions of the objects that can be cloaked. Even if the approach as such works for electrically small objects, recently some results have been presented showing how it is possible to increase the object dimensions [4]. As to the losses, this approach has the important advantage of employing homogeneous materials (i.e. there is no need to synthesize an electric/magnetic profile) possibly having a real part of the permittivity close to zero. Looking at the dispersion of the material, in fact, since the operation frequency is close to the plasma frequency and far away from the resonance of the inclusions, losses can be assumed as rather low. In addition, the dispersion curve close to the plasma frequency has a slow slope and, thus, this approach is characterized by relatively good performances in terms of bandwidth. Moreover, from the fabrication point of view, this approach leads to easier practical designs as compared to the one based on the coordinate transformation. However, some problems arise when we try to use this approach for devices working in both polarizations. For purely dielectric objects the Scattering Cross-Section (SCS) is substantially dependent on the permittivity of the cover, but for objects that exhibit also a magnetic response it's necessary to design a cover with proper values for both permittivity and permeability [1]. When trying to implement this setup at microwaves is indeed difficult to obtain such behavior with real-life inclusion-based cover. Another important issue is how to move towards optical frequencies using the same basic idea. If we would like to extend the cloaking approach proposed in [1,2] to the visible regime, we have to overcome some limitations. On one hand, in fact, the parallel plate medium cannot be used anymore at these frequencies, and, on the other hand, there is a lack of useful natural materials exhibiting the required permittivity. As previously anticipated, in fact, for materials characterized by a close-to-zero real permittivity, the plasma frequency should rest in the visible. Unfortunately, noble metals, such as gold and silver, have plasma frequencies at smaller wavelengths in the ultra-violet regime and, thus,

exhibit a strong plasmonic (i.e. the real permittivity is strongly negative) behavior in the visible. For this reason, they are not useful for such purposes as such.

Once pointed out such aspects, the aim of this study can be summarized in the following points:

1. to use homogeneous metamaterials as cloaking devices for objects of standard geometry (for example cylindrical or spherical geometry) and a given polarization; First we start with a highly idealized scenario, where we consider all materials homogeneous and high symmetry geometries. The simplicity of the approach with let us to define the materials properties needed to achieve invisibility. Later we will make use of the results obtained in this section for designing more realistic proposals.
2. to verify the possibility to use the cover for both polarizations; Any harmonic wave can be decomposed in two independent polarization states. It is therefore crucial for practical purposes to make sure that the device under study behaves as expected under illumination polarized in any of the two independent components.
3. to synthesize a cover made by real-life magnetic inclusions working in both polarization; Once the device is able to work under two defined polarization states we proceed to improve their capabilities combining the solutions found previously. The final design will then exhibit a reduced observability under any degree of polarization.
4. to realize a similar setup working at optical frequencies; One of the main goals of the study is to push forward the working wavelengths up to the visible. We will present here a proposal and discuss its performance. It is of great importance for space technology to push forward the limits of current optical systems in order to improve the performance of optical communication and astronomical spectroscopy.
5. to investigate the effects of the radiation pressure exerted on the cloaked object. An important space application of invisible devices is its ability to drastically reduce the net force exerted by the incoming radiation. On the basis of the design described in section 4 we calculate the radiation force acting on small particles and compare it with the case of a bare particle.

1 DESIGN OF INVISIBILITY CLOAKS AT MICROWAVES

In this section, we verify the possibility to use ENZ and MNZ metamaterials to design a cloaking device working in both TE and TM polarizations. At first, we recall the design principles of a cloak for the TE polarization made of an ideal homogeneous material. Then, we present the design of the same cloak implemented through real-life magnetic inclusions at microwaves and, finally, we propose the design of an actual cloaking device working for both polarizations (TE and TM) by employing both magnetic inclusions for the TE polarization and the parallel-plate medium, as proposed for the TM polarization in [2].

1.1 Cloak with ENZ materials at microwaves

When studying the propagation of a plane wave in presence of an obstacle we refer to the total field as a superposition of two electromagnetic fields: the incident field (that is the impinging field in absence of the obstacle) and the scattered field (generated by the scatterer) [14]. As figure of merit for the analysis of the electromagnetic problem we introduce the Scattering-Cross-Section (SCS, σ). In plane wave scattering the SCS is defined as the area intercepting an amount of power that, when scattered isotropically, produces at the receiver a density that is equal to the density scattered by the actual target [15]. For two-dimensional objects we denote the SCS as $\sigma_{2\text{-D}}$, while for three-dimensional objects we refer to $\sigma_{3\text{-D}}$, in formulas

$$\sigma_{2\text{-D}} = \begin{cases} \lim\limits_{\rho\to\infty}\left[2\pi\rho\dfrac{|\mathbf{E}_s|^2}{|\mathbf{E}_i|^2}\right] \\ \lim\limits_{\rho\to\infty}\left[2\pi\rho\dfrac{|\mathbf{H}_s|^2}{|\mathbf{H}_i|^2}\right] \end{cases}, \qquad \sigma_{3\text{-D}} = \begin{cases} \lim\limits_{r\to\infty}\left[4\pi r^2\dfrac{|\mathbf{E}_s|^2}{|\mathbf{E}_i|^2}\right] \\ \lim\limits_{r\to\infty}\left[4\pi r^2\dfrac{|\mathbf{H}_s|^2}{|\mathbf{H}_i|^2}\right] \end{cases}$$

where ρ, r are the distances from the object to observation point, $(\mathbf{E}_s,\mathbf{H}_s)$ and $(\mathbf{E}_i,\mathbf{H}_i)$ are respectively the scattered and incident electric/magnetic field. For cylindrical unbounded dielectric or metallic structures the scattering cross-section ($\sigma_{2\text{-D}}$) can be expressed in closed form [2,14,15,16,17], depending on the polarization (with respect to the axis of the cylinder, as shown in Fig 1). The goal is to minimize the $\sigma_{2\text{-D}}$ by using a proper designed cover surrounding the object in both the polarizations.

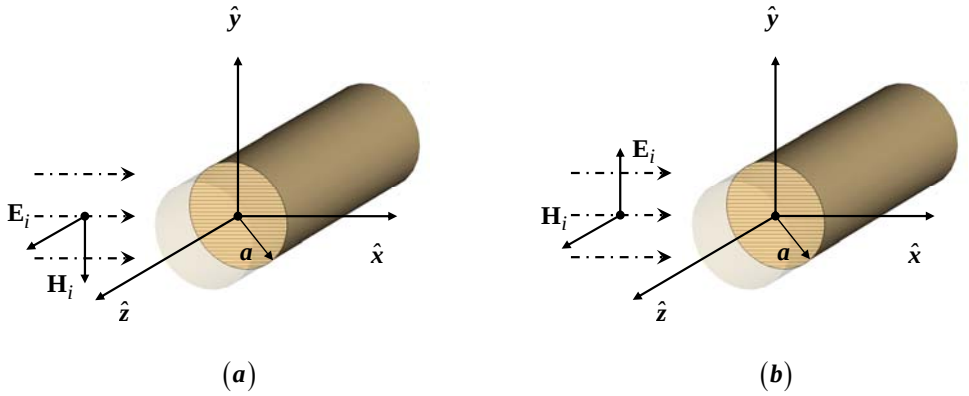

Fig. 1 Polarization of a plane wave impinging on a bare cylinder: TM (a) and TE (b) with respect to the axis of the cylinder

Even if we deal with unbounded cylinder, it'easy to describe also the case of a structure with finite length, even for oblique incidence. For example, as known from the general theory of electromagnetic scattering, in the far-field region the $\sigma_{3\text{-D}}$ of a conducting cylinder with length L is approximatively proportional to the $\sigma_{2\text{-D}}$ of the unbounded one [15,16,17]:

$$\sigma_{3\text{-D}} \approx \frac{2L^2}{\lambda}\sigma_{2\text{-D}}\, sin^2\,\theta_s\, sinc^2\left[\frac{kL}{2}(cos\,\theta_i + cos\,\theta_s)\right]$$

Now following Engheta's approach, for a cylinder of radius a and electric parameters (ε_p, μ_p) surrounded by a cover of radius b (Fig. 2) the total SCS can be numerically minimized through a proper choice of the cover permeability and permittivity in both polarizations (details in [1,2]).

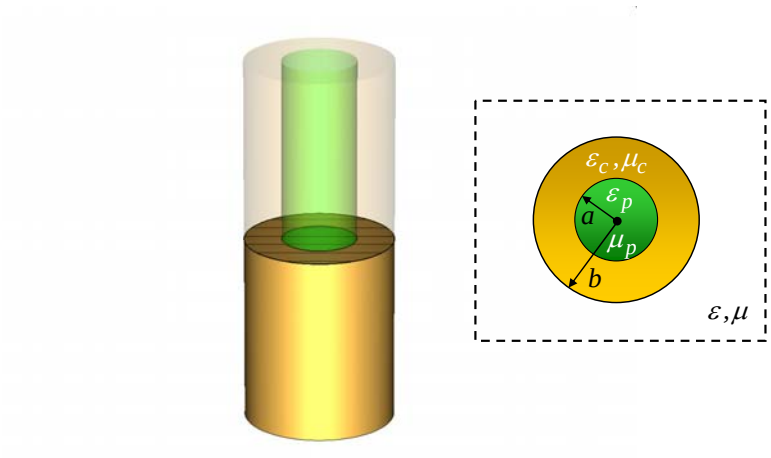

Fig. 2 Geometrical sketch of a cylinidrical object with finite length covered with a material with given costitutive parameters.

This is in ideal scenario where the cover can have arbitrary values of permittivity and permeability, independently from the frequency or losses. Using Engheta's design formulas [1,2], we try to numerically minimize the SCS. We choose, as example, to reduce the observability of a cylindrical object with the electric and geometric parameter

$$\begin{cases} a = 10\ \text{mm} \\ b = 1.8\,a \\ \varepsilon_p = 2 \\ \mu_p = 2 \end{cases}$$

at the operating frequency $f_0 = 3\ \text{GHz}$ ($\lambda = 10\ \text{cm} = 10\,a$), an ENZ cover material is needed in order to reduce the SCS for the TM polarization. The cover material parameters are numerically found to be $\varepsilon_c = 0.1$, $\mu_c = 1$. In order to show the results in a proper way, we introduce the ratio σ_{TM} between the total scattering cross-sections of the bare object and of the object with the cloak put on it. The theoretical minimization rate of the SCS for a homogeneous ideal lossless cover is shown in Fig 3.

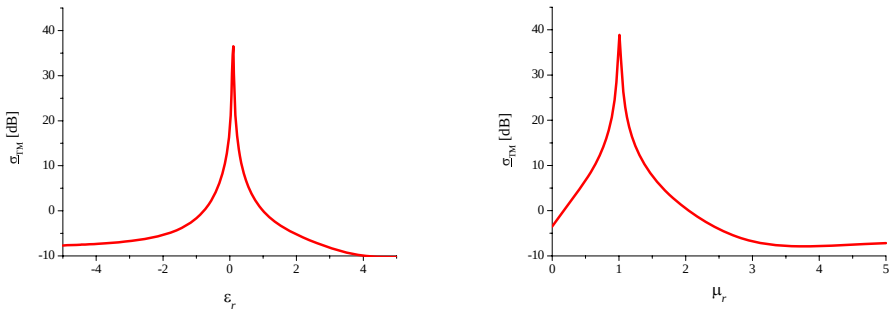

Fig. 3 Theoretical minimization rate of the SCS for a variation of the cover electrical parameters

In a more realistic scenario we consider now dispersive materials with a Drude-like behavior and low losses, using the following dispersion:

$$\varepsilon_{eff}(\omega) = \varepsilon_\infty + \frac{\omega_p^2}{\omega(\omega - j\nu_c)} \qquad \begin{cases} \omega_p = 2\pi 3\times 10^9 \\ \varepsilon_\infty = 1 \\ \nu_c = 2\pi 3\times 10^7 \end{cases}$$

The SCS minimization is still achieved at the design frequency (see Fig. 4), but the dispersion determines a bandwidth due to the variation of the permittivity from its design value (Fig. 3).

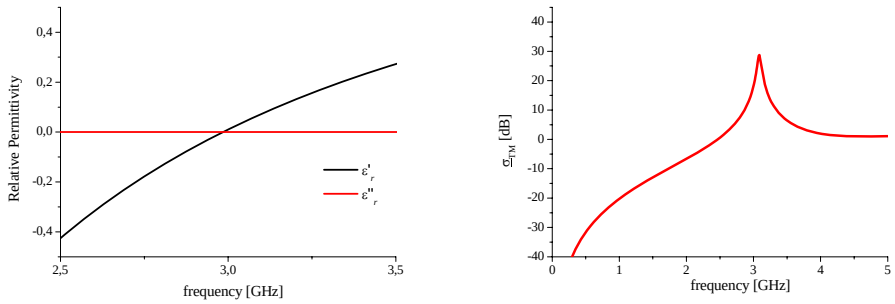

Fig. 4 Theoretical SCS minimization rate for a Drude-like dispersive permittivity.

Even increasing the losses a good minimization rate can still be obtained, as shown in Fig. 5, where the real part ε_c' of the relative permittivity $\varepsilon_c = \varepsilon_c' - j\varepsilon_c''$ of the cover material is kept unchanged and equal to the design value, while the imaginary part ε_c'' is progressively increased. Anyway, since the ENZ regime is considered, losses are expected to be low. Looking at the dispersion of the material, in fact, since the operation frequency is close to the plasma frequency and far away from the resonance of the inclusions, losses can be assumed as rather low. In addition, the dispersion curve close to the plasma frequency has a flatter slope and, thus, this approach is characterized by relatively good performances in terms of bandwidth.

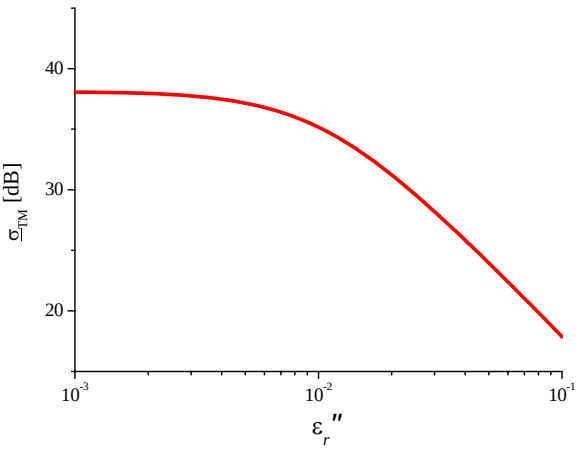

Fig. 5 Theoretical SCS minimization rate versus losses in the metamaterial cover.

The approach is shown to be robust with variation of the geometrical dimensions of the cover, as quite evident in Fig. 6, where is depicted the variation of σ_{TM} keeping all the setup parameters to their design values and varying only the radius of the external cover.

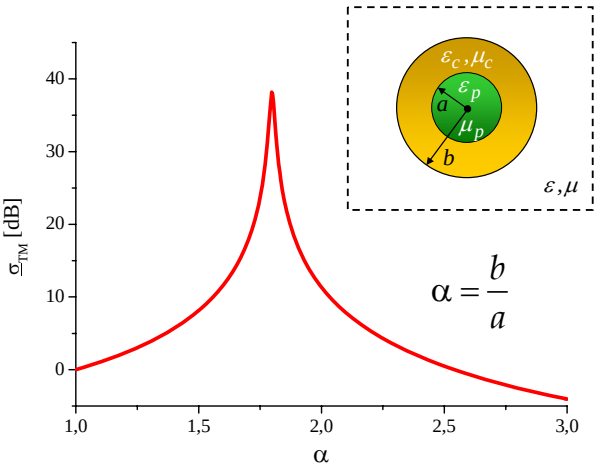

Fig. 6 Theoretical SCS minimization rate versus geometrical parameters.

1.2 Cloak with MNZ materials at microwaves

For the same cylindrical object, an MNZ material is needed in order to reduce the SCS for the TE polarization. In fact, as expected by duality, we numerically found the following values for the constitutive parameters: $\varepsilon_c = 1, \quad \mu_c = 0.1$. The theoretical minimization rate σ_{TE} of the SCS for a homogeneous ideal lossless cover is shown in Fig 7.

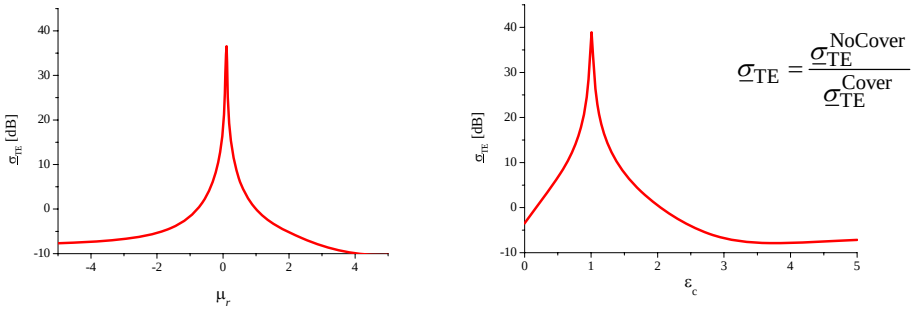

Fig. 7 Theoretical minimization rate of the SCS for a variation of the cover electrical parameters.

Then we consider an ideal isotropic and homogeneous material having the relative permittivity equal to one and a permeability following the Lorentz model (Fig. 8). The Lorentz model parameters are the following

$$\mu_{eff}(\omega) = \mu_\infty + \frac{(\mu_s - \mu_\infty)\omega_0^2}{\omega_0^2 + j\omega\delta - \omega^2} \qquad \begin{cases} \mu_s = 2 \\ \mu_\infty = 1 \\ \omega_0 = 2\pi\, 2.065 \times 10^9 \\ \delta = 2\pi\, 2 \times 10^7 \end{cases}$$

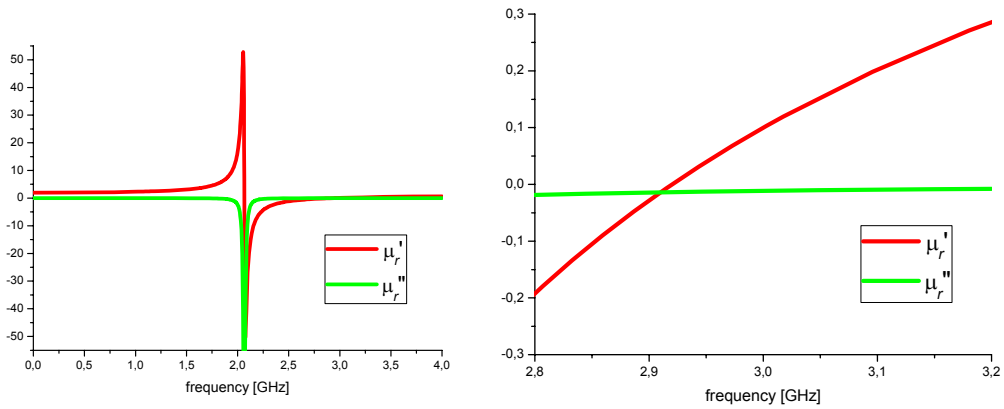

Fig. 8 Lorentz dispersion for permeability (left) and a zoomed view close to the design frequency (right).

Such materials can be obtained practically implemented at microwaves using metallic inclusion [18,19]. The SCS minimization is shown in Fig. 9, it is worth noticing that, as expected, at the resonant frequency of the permeability (around 2 GHz) the scattering cross-section of the object with the cover is very much increased compared to the one of the bare object. At lower frequencies the Lorentz model has real part of the permittivity that approaches μ_s, so the SCS is rather constant. The Drude model instead has a real part diverging when the frequency goes to zero, determining the profile shown in Fig. 4.

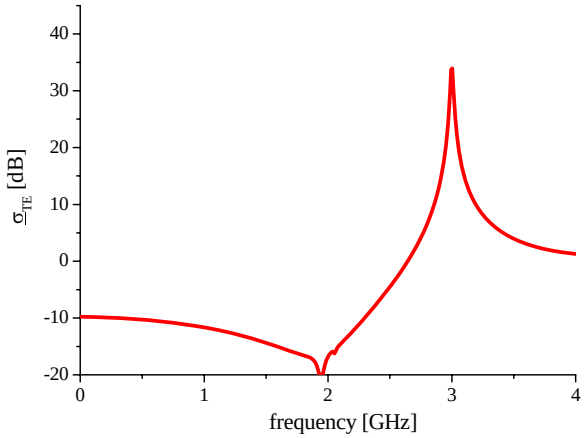

Fig. 9 Theoretical SCS minimization rate for a Lorentz-like dispersive permittivity.

Even in this polarization the robustness to losses and geometrical variation is rather acceptable near the operating frequency (see Figs. 10-11).

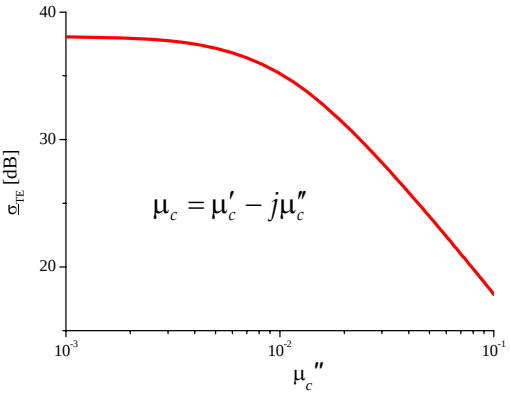

Fig. 10 Theoretical SCS minimization rate versus losses in the metamaterial cover.

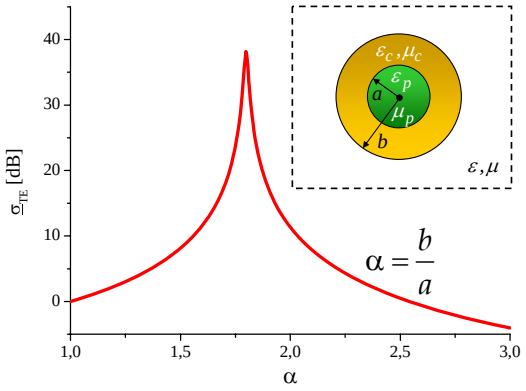

Fig. 11 Theoretical SCS minimization rate versus geometrical parameters.

As in the other polarization, the variation of σ_{TE} in Fig. 10 is obtained varying only the imaginary part of the design permeability, and in Fig. 11 keeping all the setup parameters to their design values and varying only the radius of the external cover.

1.3 *Full wave simulations of an ideal MNZ-ENZ cloak at microwaves*

We present here some full wave simulations of the theoretical structures presented so far. Calculations have been performed through a finite integration technique (FIT) code [20]. First of all we have checked the behavior of an ideal cloak for the TM polarization. A plane wave has been supposed to impinge on a cylinder of length *L* covered with a dispersive homogeneous cloak (see Fig. 12).

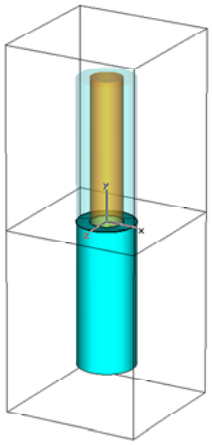

Fig. 12 *Simulation layout of a cylindrical object covered with an ideal cover. The structure has open boundaries.*

The σ_{TM} has been computed for different values of *L*, keeping all the parameters at their design values and varying only the cylinder length, as is shown in Fig. 13.

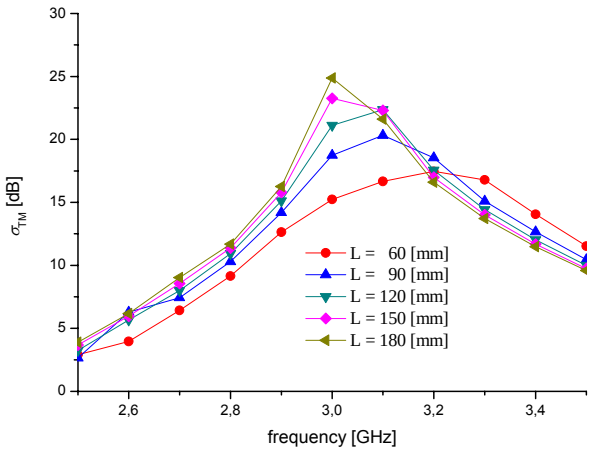

Fig. 13 *SCS minimization rate versus cylinder length.*

The observability of the cylinder is not reduced as much as in the infinite case, but, as previously anticipated, when we increase the length of the cylinder, the results should approach those ones of the unbounded structure. The obtained effective bandwidth is clearly consistent with the ideal behavior shown in Fig. 4: when we move from the cover permittivity design frequency, σ_{TM} decreases due to the mismatch of the electric parameters. The ideal gain obtained in a certain frequency range shown in Fig. 4 is now also a function of the cylinder length, so for larger values of *L* higher values of σTM are obtained. In Fig. 14 we plot instead the maximum of SCS (the SCS is a function of angular coordinates, so the maximum is chosen as the greatest value in magnitude assumed between all directions [1,14,15,16,17]), versus frequency of both the bare cylinder and the cloaked one. Finally in Fig. 15 we present the variation of the reduced observability figure of merit σ_{TM} with the length *L* of the cylinder at the cloaking frequency.

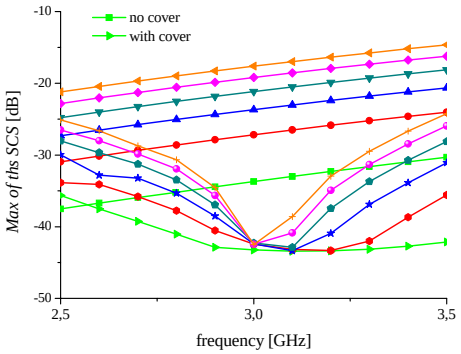

Fig. 14 *Comparison of the maxima of the SCS versus the cylinder length for the bare cylinder and the covered one.*

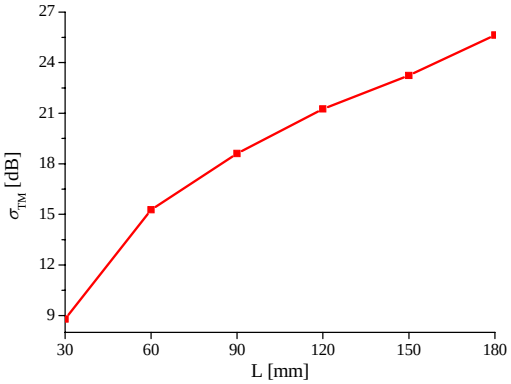

Fig. 15 *SCS minimization rate versus cylinder length at cloaking frequency.*

The response to variations of the geometric parameters is shown in Fig. 16, where is depicted the minimization rate at cloaking frequency for different values of the ratio α. The plot is obtained keeping all the parameters to their design values and varying only the external cover radius (see Fig. 16).

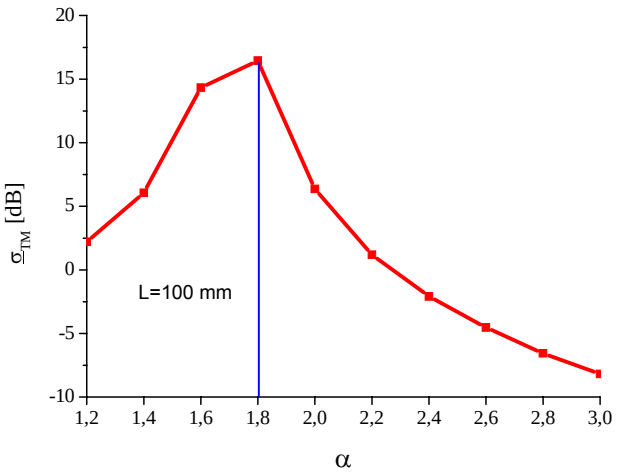

Fig. 16 *SCS minimization rate at cloaking frequency for different values of the ratio α.*

The scattering reduction is clearly evident in the 3D plot of the SCS and in the amplitude of the electromagnetic field across the obstacle. The comparison between the case of the bare cylinder and the covered one, both with *L* = 200 mm, is shown in Fig. 17.

In Figs. 18-19 we present, instead, the distribution of the electric and magnetic fields, respectively, in the case of both bare and covered objects.

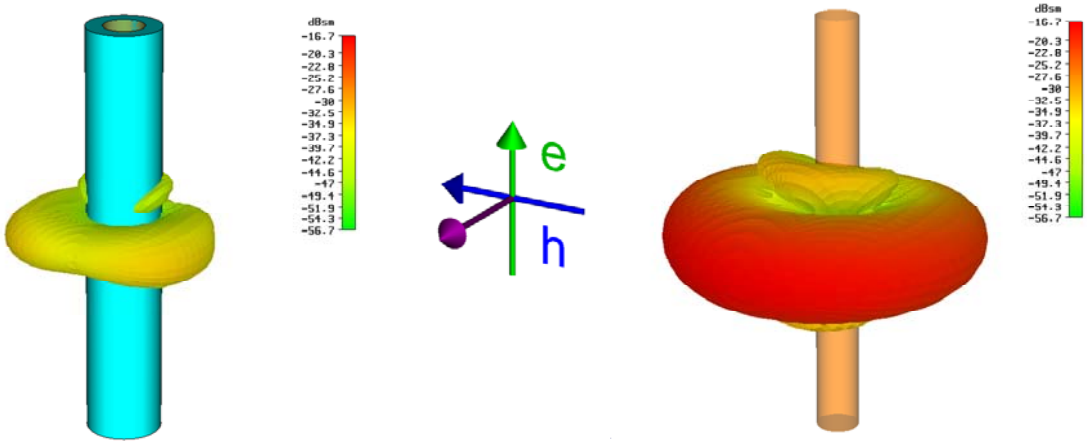

Fig. 17 *SCS for a cylinder with (left) and without (right) the cover.*

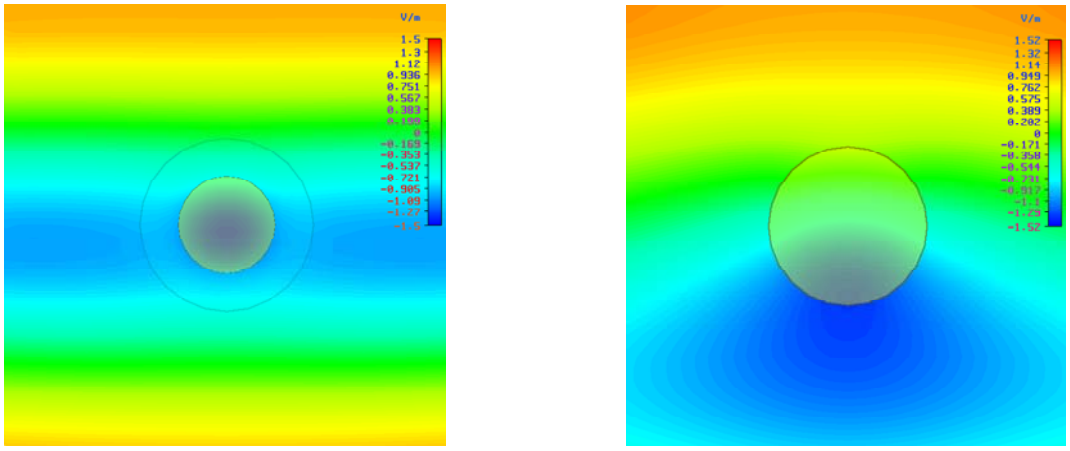

Fig. 18 Electric field for a cylinder with (left) and without (right) the cover.

In the case of the bare cylinder, the shadow effect is very evident, while in the covered case it is reduced, though the field is not perfectly uniform. While in the first case the field lines are deformed by the presence of the obstacle, in the second one they are more similar to the field lines of a plane wave travelling unaltered through the object.

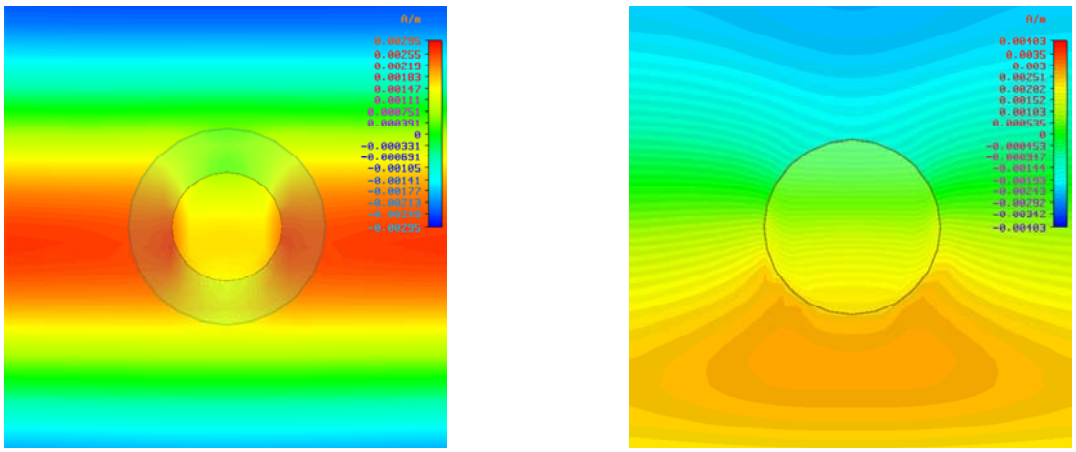

Fig. 19 Magnetic field for a cylinder with (left) and without (right) the cover.

The corresponding results for TE polarization are shown in Figs. 20-25, the same considerations can be done simply applying duality.

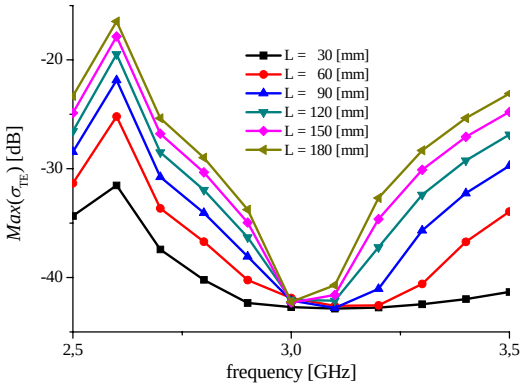

Fig. 20 Maximum of the SCS versus cylinder length in the case of covered cylinder.

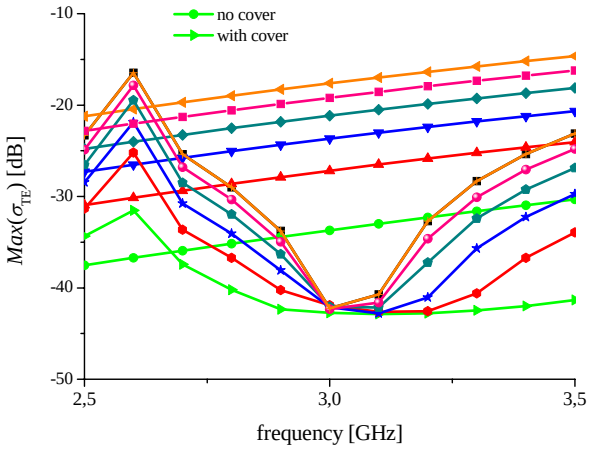

Fig. 21 Comparison of the maxima of the SCS versus cylinder length for the cases of bare and covered cylinder.

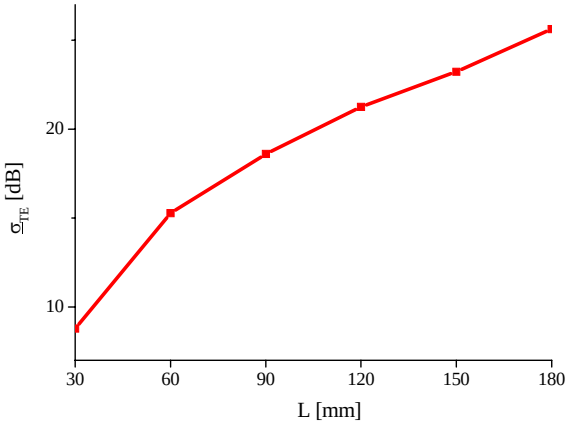

Fig. 22 SCS minimization rate versus cylinder length at cloaking frequency.

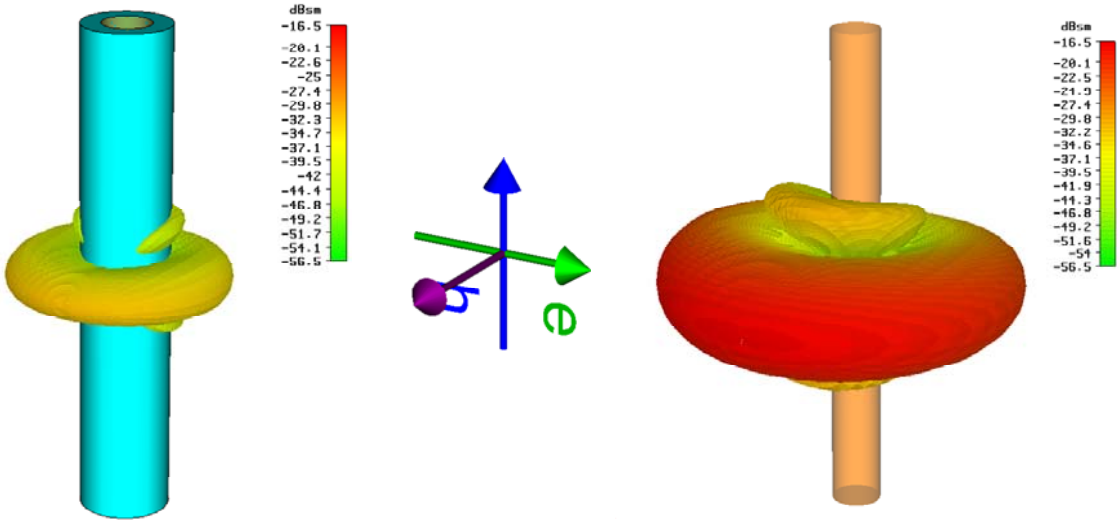

Fig. 23 *SCS for a cylinder with (a) and without (b) the cover.*

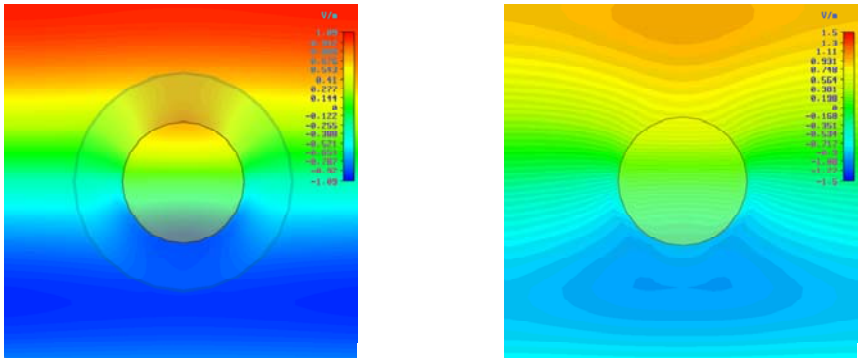

Fig. 24 *Electric field for a cylinder with (left) and without (right) the cover.*

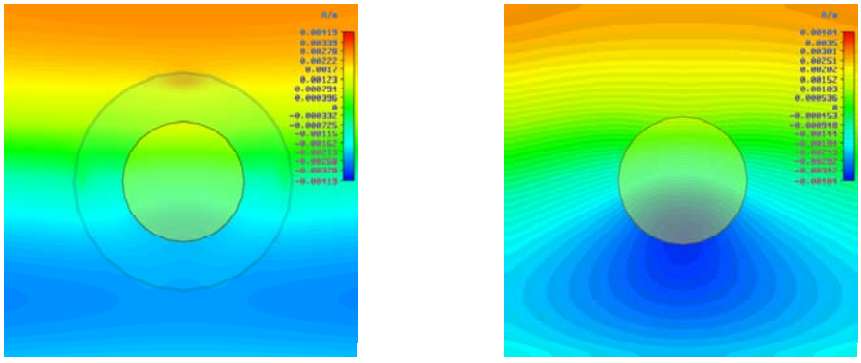

Fig. 25 *Magnetic field for a cylinder with (left) and without (right) the cover.*

1.4 *Design of an MNZ-ENZ cloak at microwaves with magnetic inclusions*

In this section we extend the previous results in order to synthesize a device working in both the fundamental polarization. We need to design a structure with MNZ behavior for TE polarization and ENZ behavior for TM polarization. For the first one we present a real life implementation of the MNZ cover using magnetic inclusions. In order to obtain the desired value of the permeability for the cover material, we have used the spiral resonators (SRs), following the design presented in [18,19]. We choose to use of SRs here because they have a higher miniaturization rate [18,19] respect to standard split ring resonators. The inclusions, in fact, have to be put in the space delimited by the external cover radius and the object radius. The object considered in this example is again a cylinder with radius a = 10 mm and length L = 50 mm, made of a material with constitutive parameters given by $\varepsilon = 2\varepsilon_0$ and $\mu = 2\mu_0$. In order to design the MNZ cover we have considered four columns of SRs disposed as shown in figure 9a. The single SR inclusion has two turns and an external length of l_{SR} = 3.5 mm, the separation between two adjacent turns is 0.6 mm, while the metallic strip has a width of 0.3 mm. ENZ materials can be realized at microwaves with the parallel plate Rotman medium, following the design proposed in [2] The spiral resonators must be necessary placed along the structure with the plane containing the metallization parallel to the cylinder cross-section, in order to be properly excited by the magnetic field in TE polarization (Fig. 26)

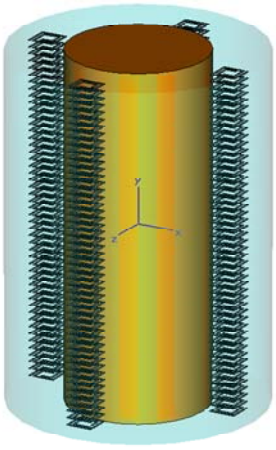

Fig. 26 *Simulation setup with spiral resonators disposed around the cylinder.*

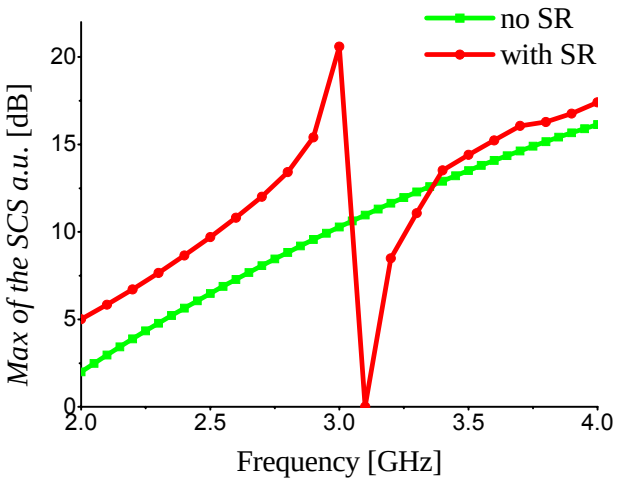

Fig. 27 Maximum of the SCS in the case of the bare and covered object.

Exciting the structure through the same plane wave as in the previous section and performing full-wave simulations we obtained the results shown in Fig. 27. The reduction of the object observability around the desired frequency is well evident. In addition, as expected, at the resonant frequency of the SRs the covered structure scatters strongly and, thus, the observability of the object is indeed increased. Far from the resonance of the SRs and the design frequency, then, the scattering cross-section of the covered object approaches the one of the bare cylinder. The pattern of the scattering cross-section (Fig. 28) clearly shows that the dominant scattering term for the bare cylinder[1] is the dipolar one, due to its electrically small dimensions. When the cloak is working the dipolar term is almost suppressed and the higher order terms, which have significantly lower amplitude, become the dominant ones.

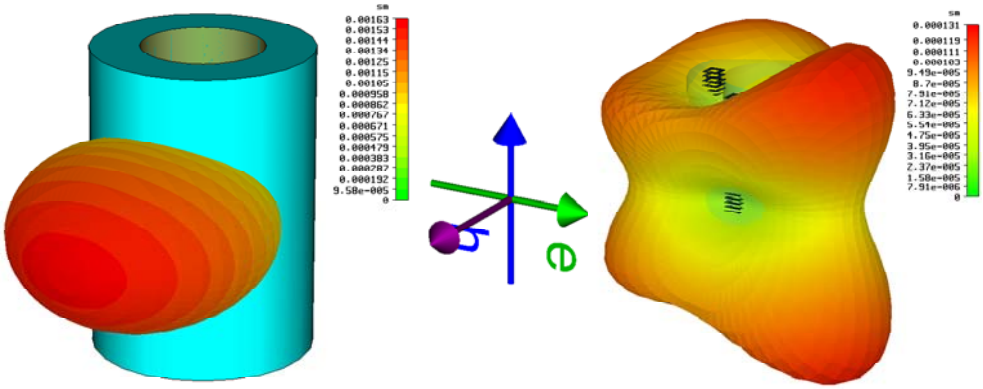

Fig. 28 SCS of a cylinder with (right) and without (left) the SRs.

[1] The blue cover is a vacuum cover introduced for convenience

We report in Fig. 29-30 also the bi-dimensional plots showing the electric and magnetic field pattern at the cloak frequency in the cases of bare and covered cylinders. In the case of the bare cylinder, the shadow effect is very evident, while in the covered case it is reduced, though the field is not perfectly uniform. This is mainly due to the fact that we have used only four columns of SRs here. The reason of this choice is that, in order to host the inclusions of the magnetic kind working for the TE polarization, in the layout based on the parallel plate medium and working for the TM polarization, it is necessary to reduce the number of the plates to leave room to the SRs.

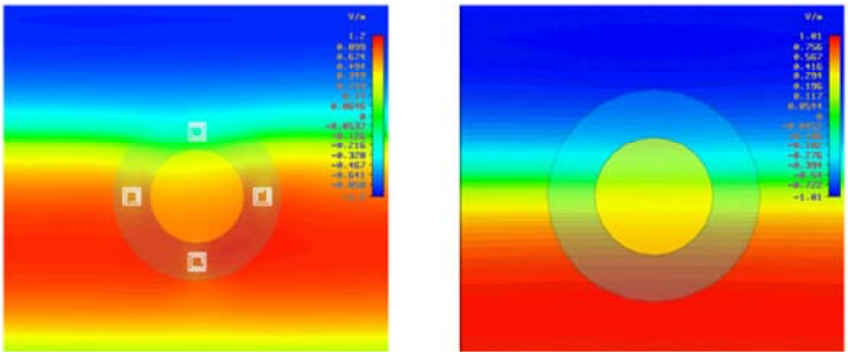

Fig. 29 *Electric field for a cylinder with (left) and without (right) the SRs cover.*

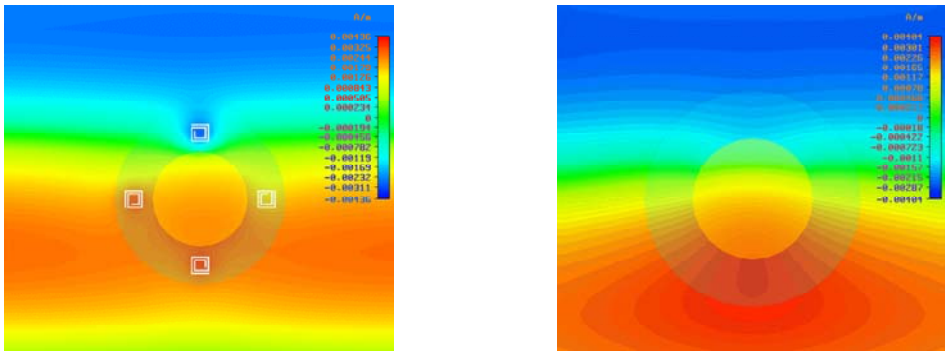

Fig. 30 *Magnetic field for a cylinder with (left) and without (right) the SRs cover.*

Extracting through a standard method based on the reflection and transmission coefficients [21,22] the permeability function of the four columns of SRs when the same TE plane wave impinges on the structure is evident that at the frequency at which the cloak works, the value of the effective relative permeability of the cover is close to zero (see Fig. 31).

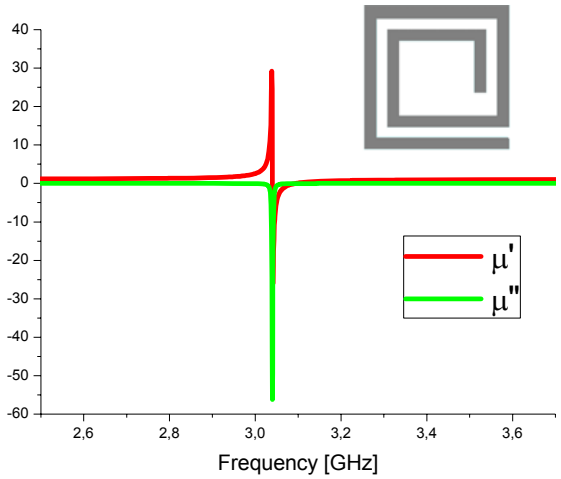

Fig. 31 *Permeability function of the four columns of SRs extracted from reflection coefficients.*

Moreover, in Fig. 32 it is shown that, when increasing the size of the SRs, the cloaking frequency shifts towards lower values, being lower the frequencies at which the corresponding effective permeabilities exhibit values close to zero.

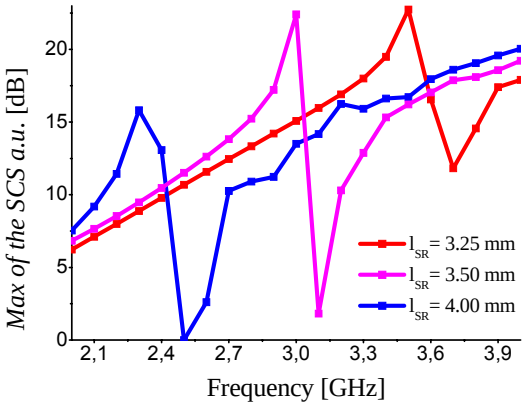

Fig. 32 *Maximum of the scattering cross section of the covered cylinder versus frequency for different values of the SRs size.*

As noticed previously in order to obtain a cloaking device working for both TM and TE polarizations, we should mix up the design we have here proposed for the TE polarization with the one based on the employment of the parallel plate medium. In this case the reduced number of both plates (four) and SR columns (four) does not lead to an optimal design for either polarization. Anyway, the interesting advantage of this setup is that this cloaking device works now for both polarizations, as it is evident in Fig 33.

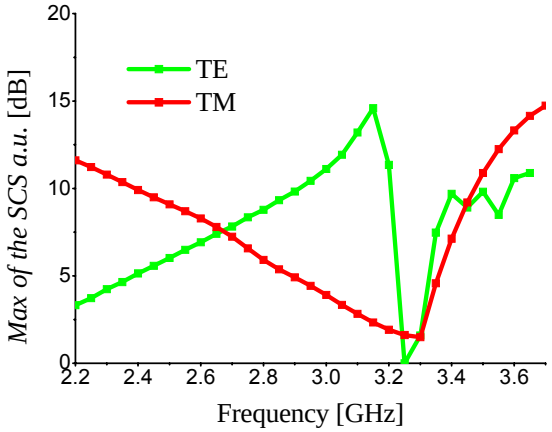

Fig. 33 Maximum of the SCS in the case of the bare and covered object.

2 DESIGN OF A CLOAK WITH ENZ METAMATERIALS AT THZ AND/OR OPTICAL FREQUENCIES

Metals exhibit a real negative permittivity in the visible. Layered structures realized with a stack of alternating plasmonic and dielectric slab can exhibit an ENZ behavior in the visible range [23]. If the thicknesses of the slabs are electrically small, the resulting composite material is described through constitutive parameters depending only on the ratio between the thicknesses of the labs and the constitutive parameters of the two different materials.

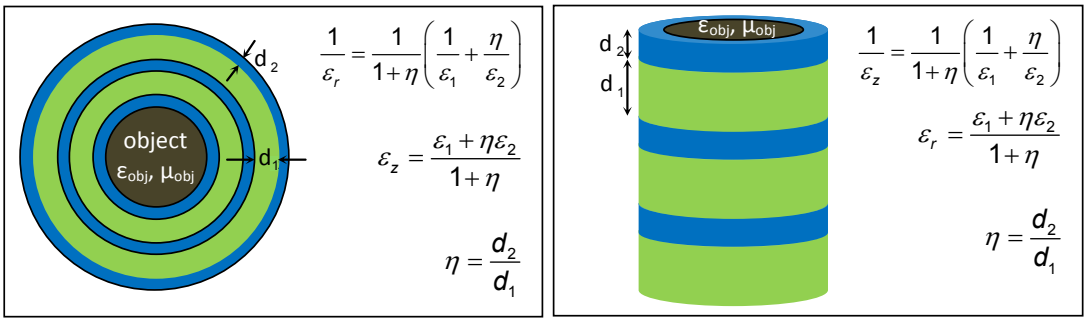

Fig. 34 Sketch of the layered medium cylindrical cover.

It is possible to stack the two materials in two different ways. In both cases, the resulting composite material is anisotropic and the expressions of the entries of the permittivity tensor are given in the insets of the Fig. 34. With a plasmonic material like silver and silica it is possible to obtain an ENZ material along the axis of the cylinder in the visible (see Fig. 35).

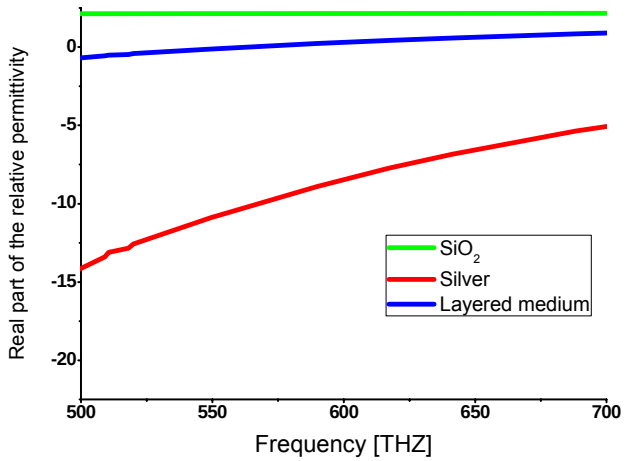

Fig. 35 Frequency dispersion for the proposed layered medium.

Using this kind of design for a dielectric cylinder with parameters

$$\begin{cases} a = 50 \text{ nm} \\ b = 1.8\, a \\ \varepsilon_p = 2 \\ \mu_p = 1 \end{cases}$$

at the operating frequency $f_0 = 600$ THz ($\lambda = 0.5\ \mu\text{m} = 10\, a$), we obtained the following geometric values for the cover with radial concentric shells with an impinging wave TM polarized (i.e. the electric field is along the axis of the cylinder)

$$\begin{cases} \eta = 0.21 \\ d_1 = 10 \text{ nm} \\ \varepsilon_c \approx 0.22 \end{cases}$$

Full wave simulations for TM polarization are shown in Figs. 36-37. The reduction of the object observability around the desired frequency is quite evident. As expected, below the plasma frequency the observability of the object is partially increased due to the strong plasmonic behavior of the Ag, while at higher frequencies the SCS of the covered object approaches the one of the bare cylinder.

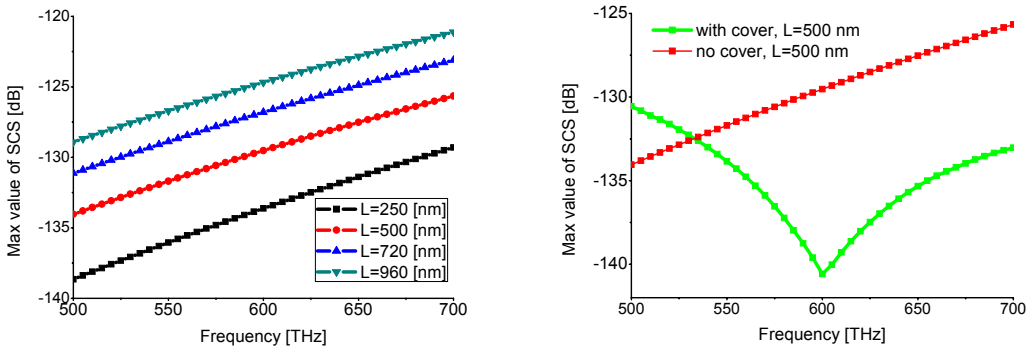

Fig. 36 *Maximum of the SCS versus cylinder length in the case of bare (left) and covered (right) cylinder.*

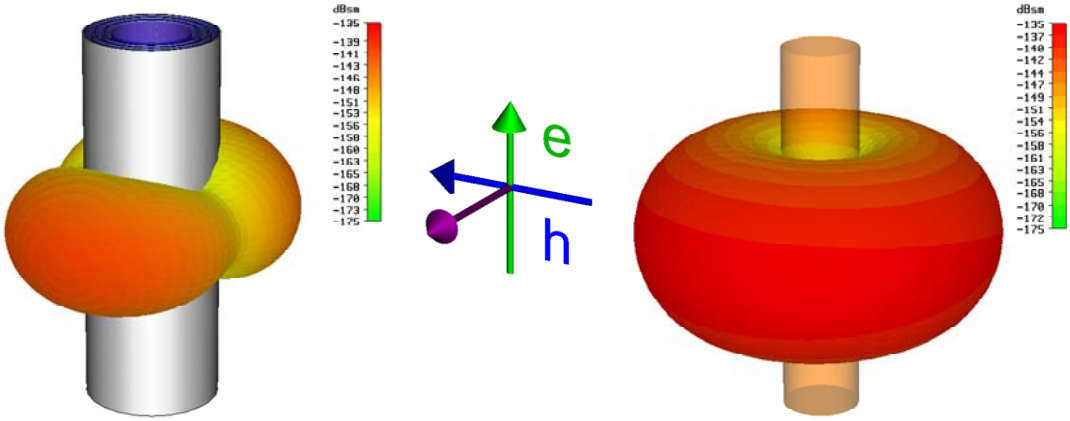

Fig. 37 SCS for covered (left) and uncovered (right) dielectric cylinder.

Looking at the bi-dimensional plots of the electric and magnetic field amplitude distributions at the cloak frequency (Figs. 38-39), the shadow effect is well evident in the case of the bare cylinder, while in the covered case it is visibly reduced.

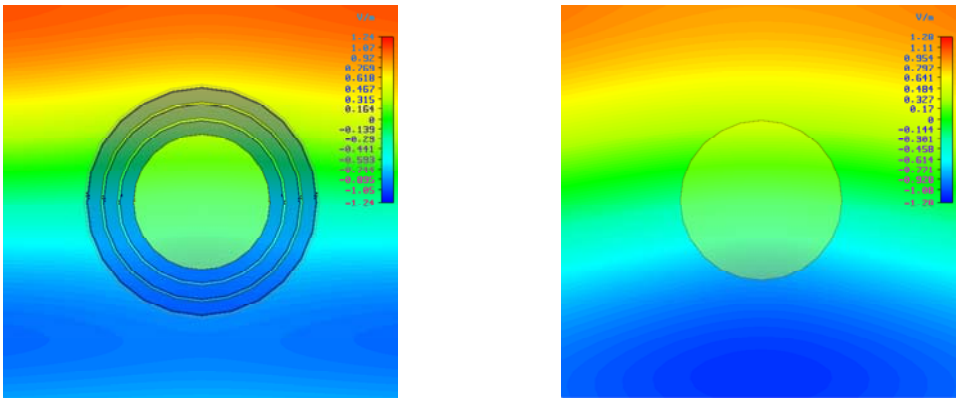

Fig. 38 Electric field for a cylinder with (left) and without (right) the cover.

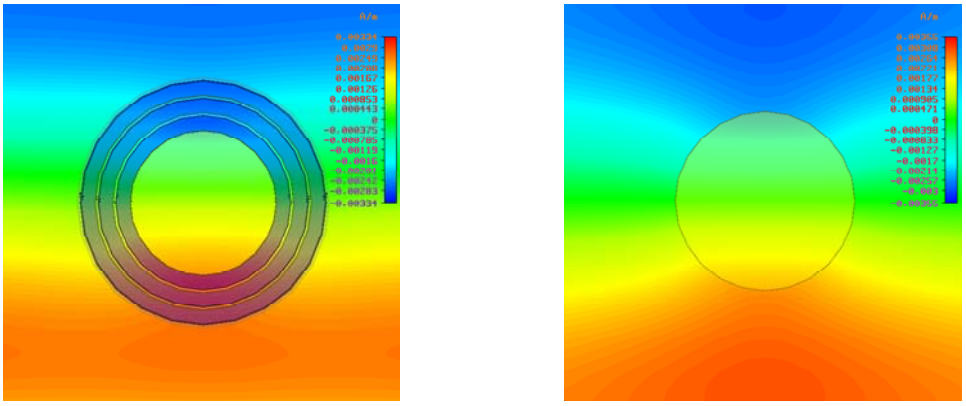

Fig. 39 Magnetic field for a cylinder with (left) and without (right) the cover.

The same approach can be used also to cloak an object with magnetic properties. Even if in the visible regime there are no natural materials exhibiting a magnetic response, some interesting new results are being obtained in this field with artificial materials [24]. For an object exhibiting magnetic properties at the operating frequency $f_0 = 600$ THz, we consider the following example

$$\begin{cases} a = 50 \text{ nm} \\ b = 1.8\, a \\ \varepsilon_p = 2 \\ \mu_p = 2 \end{cases}$$

This time we found the design permittivity to be $\varepsilon_c = 0.1$, $\mu_c = 1$, with the geometric parameters:

$$\begin{cases} \eta = 0.23 \\ d_1 = 10 \text{ nm} \end{cases}$$

Full wave simulations for TM polarization are shown in Figs. 40-43.

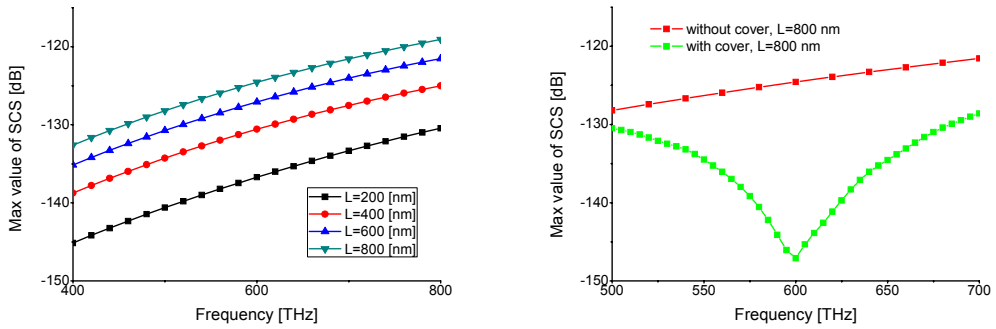

Fig. 40 Maximum of SCS for different cylinder lengths

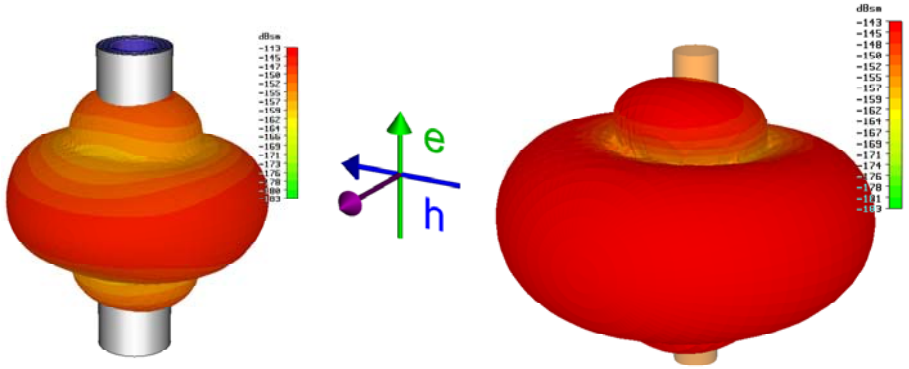

Fig. 41 SCS for uncovered (left) and covered (right) cylinder.

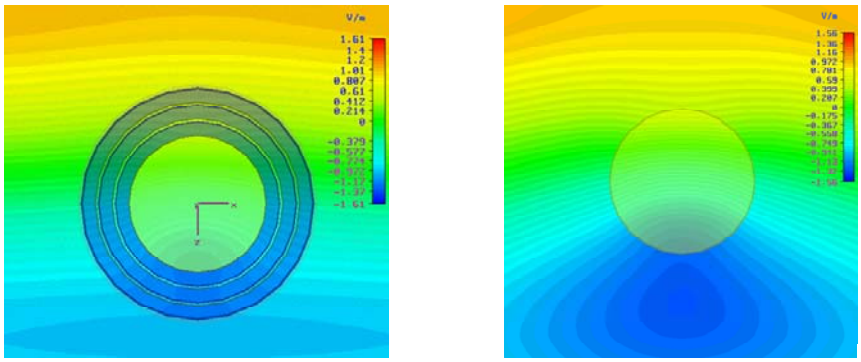

Fig. 42 Electric field for a cylinder with (left) and without (right) the cover.

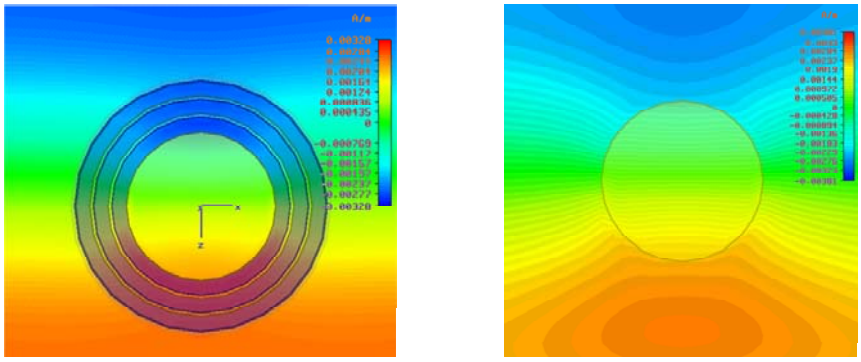

Fig. 43 Magnetic field for a cylinder with (left) and without (right) the cover.

For covered spherical particles the normalized SCS can be expressed through Mie theory like in the cylindrical case, obtaining in the Rayleigh limit a closed from for the scattering coefficients [14,15,16,17].

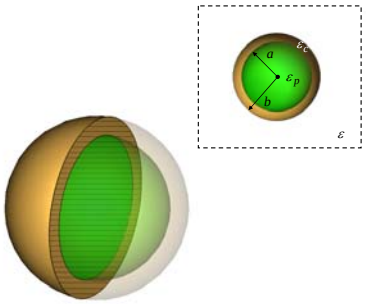

Fig. 46 Sketch of a covered spherical particle.

Following the same approach used in the cylindrical geometry, the layered medium can be employed also in this geometry. Due to the anisotropic behaviour of the layered medium (e.g. we cannot have here the same values for the diagonal elements of the permittivity tensor), it is impossible to have a cloaking device working for both TM and TE polarizations at the same frequency. In the case of spherical layered structures, we could consider two

different ways to stack the two materials. One possibility is to use concentric spherical shells and the other one is to use a stack of annular circular slices following the profile of the sphere. Anyway, the first setup is only suited for an impinging wave having a radial electric field. In the design reported in Fig. 47, we have, accordingly, stacked the different material slices along the direction orthogonal to the incident electric field. The operation of such configuration is substantially independent from the electric field direction in the plane of the layers, while we expect that the cloak should not work for the orthogonal polarization.

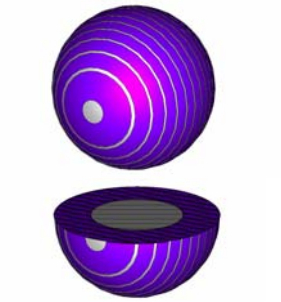

Fig. 47 Layered cover for spherical particles.

In order to validate the theoretical result we have performed some full-wave simulations with typical setups. Let's consider a spherical particle made of Ag (whose dispersion was previously shown in Fig. 35) with radius a = 50 nm. Again, we use the homogeneous cover approach in order to synthesize a spherical shell with a proper permittivity value. For a homogenous dielectric spherical shell with radius b = 1.8 a working at the frequency f_0 = 600 THz the required relative permittivity is $\varepsilon_c = 0.5\varepsilon_0$. Applying the design formulas reported in the inset of Fig. 10b and using again alternating layers of SiO_2 with thickness d_1 = 10 nm and Ag, the optimal value for the thickness ratio is found to be η = 0.2. In Fig. 48 it is shown the maximum of the SCS of the Ag spherical shell with and without the cloak.

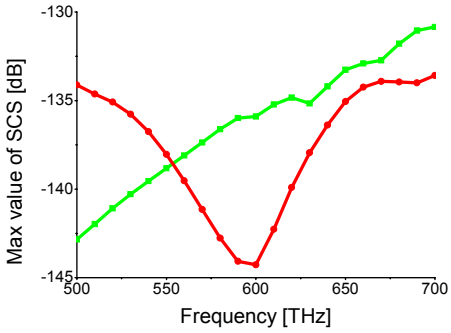

Fig. 48 Maximum of the SCS for a silver covered particle.

The sensitivity of the cloaking device with the variations of the geometrical parameters is shown in Fig. 49. As expected, a reduction of the ratio between the layer thicknesses corresponds to a lower-shift of the cloak operation frequency. Since the permittivity of SiO_2 is almost constant with the frequency, in fact, when lowering η, a higher (negative) value of the permittivity is required. The needed value can be found in the Ag dispersion at lower frequencies

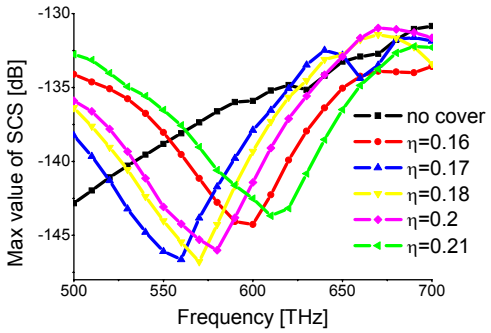

Fig. 49 Maximum of the SCS for different sizes of the stacked layers.

As previously anticipated, the proposed setup is clearly independent from the orientation of the electric field in the plane of the layers, while it expected not to work when the electric field is orthogonally directed with respect to the layers. In Fig. 50, we present the SCS of the same spherical particle used in the previous examples for differently polarized incident plane waves. When the electric field is orthogonal to the layers, the cloaking effect disappears, because the effective permittivity seen by the impinging wave (i.e. the orthogonal component of the permittivity) does not match the design value. In addition, since this permittivity is greater than ε_0, the total SCS is even bigger than the one of the bare silver sphere

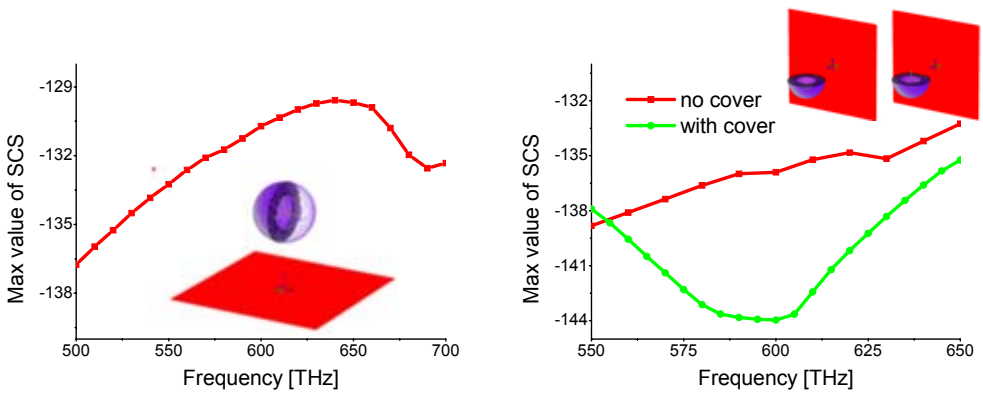

Fig. 50 Maximum of the SCS for a covered silver sphere for different polarizations.

The bi-dimensional plots of the electric and magnetic field amplitude distributions at the design cloak frequency are reported in Figs. 51-52. From these graphs, it is well evident that in the case of the covered sphere the fields are noticeably less perturbed.

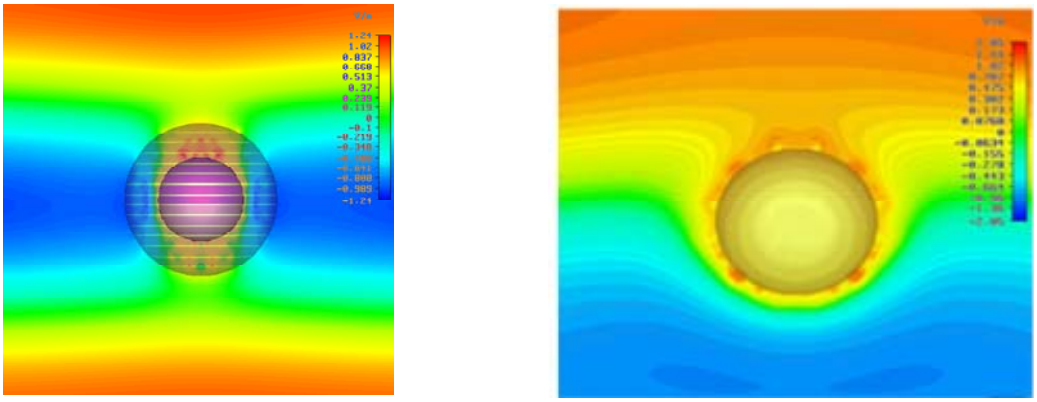

Fig. 51 Electric field for a silver sphere with (left) and without (right) the cover.

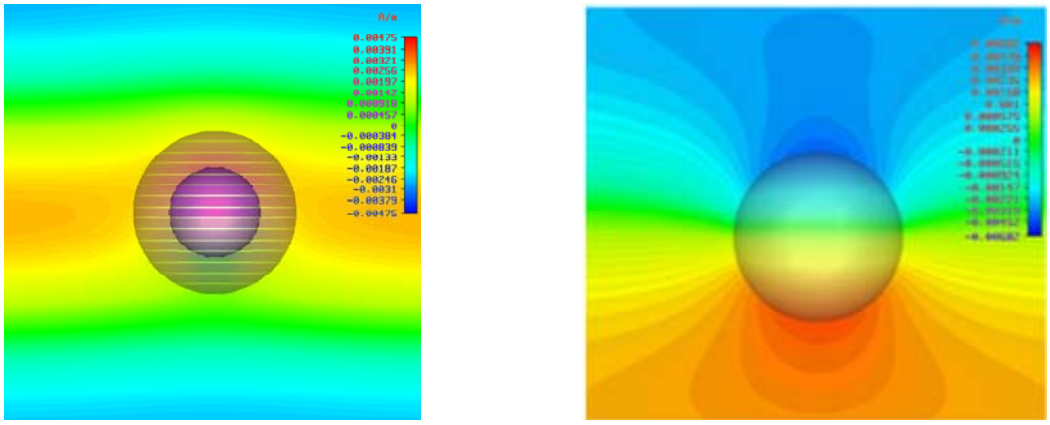

Fig. 52 Magnetic field for a silver sphere with (left) and without (right) the cover.

3 REDUCTION OF THE RADIATION PRESSURE BY OPTICAL CLOAKING

Optical forces on illuminated particles can be deduced from the Lorentz law or Maxwell stress tensor [25-29]. Typically these forces are distinguished in gradient forces that move particles towards the spots of light intensity, and scattering forces, explained by the transfer of momentum between the electromagnetic waves scattered by the particle and the particle itself. This topic is of great relevance for space. When the size of a particle is smaller than ~1 μm, the dominant force acting on it is not the gravitational one, but the solar radiation pressure and the Lorentz force[2] [30]. Moreover, in a long term, the control on the solar pressure can open the possibility to new mission, where the position of the satellites must be controlled in a highly accurate way. As pointed out in some recent papers [25] in 2D lossless problems with TM polarization light, these scattering forces can be derived from a scalar potential (that is they reduce to gradient forces), and the elementary optical forces inside are directed towards the smallest values of the potential, that is the spots of electric power density. In this case the force general expression [25] for lossless dielectrics is

$$\mathbf{f}_{xy} = \int_{\Omega} -\nabla U d\Omega + \frac{(\varepsilon - \varepsilon_0)}{2} \int_{\partial\Omega} Re\left[E_n^{in} \mathbf{E}_{t,xy}^{*} \right] d\partial\Omega + \frac{\left(\varepsilon^2 - \varepsilon_0^2\right)}{4\varepsilon_0} \int_{\partial\Omega} \left| E_n^{in} \right|^2 \mathbf{n} d\partial\Omega$$

$$\mathbf{f}_z = \frac{1}{2\omega} \frac{(\varepsilon_0 - \varepsilon)}{4\varepsilon} \int_{\partial\Omega} Im\left[\hat{\mathbf{z}} \left(\nabla H_z \times \nabla E_z^{*} \right) \right] d\partial\Omega + \frac{(\varepsilon - \varepsilon_0)}{2} \int_{\partial\Omega} Re\left[E_n^{in} \mathbf{E}_z^{*} \right] d\partial\Omega$$

$$U = \frac{1}{4}\left(1 - \frac{\varepsilon_0}{\varepsilon}\right)\left(\mu_0 \left|H_z\right|^2 - \varepsilon \left|E_z\right|^2\right)$$

that for TM (respect to cylinder axis) polarization ($H_z = 0$) simplifies to:

$$\mathbf{f}_{xy} = \int_{\Omega} -\nabla U d\Omega = \int_{\Omega} \frac{1}{4}(\varepsilon_0 - \varepsilon) \nabla \left|E_z\right|^2 d\Omega$$

$$f_z = 0$$

$$\bar{\mathbf{f}} = \frac{\omega\mu_0}{2} Im\left[\mathbf{P} \times \mathbf{H}^{*} \right], \quad \mathbf{P} = (\varepsilon - \varepsilon_0)\mathbf{E}_z$$

being $\bar{\mathbf{f}}$ the force density. In Fig. 44 is shown the total force exerted on an electrically small (*a* = 12.5 nm) dielectric (relative permittivity ε_r) lossless

[2] Interaction between any eventually charge of the particle with the planetary magnetic fields.

cylinder illuminated by a plane wave. The calculations have been performed expanding the fields in the previous equations in cylindrical functions according to scattering theory [14,15,16,17], and truncating the series expansion of the electric field using the approximation of electrically small dimensions. The force goes to zero when the cylinder has a relative permittivity near to one (cylinder made of the same material of surrounding space) or zero (static limit).

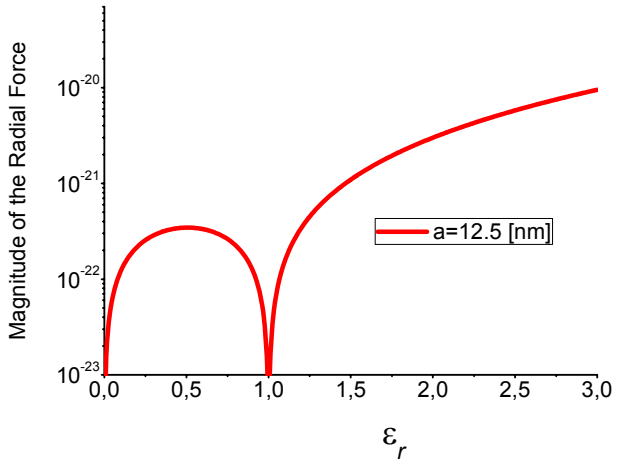

Fig. 44 Total force exerted on dielectric lossless cylinder illuminated by a plane wave.

The force exerted on a covered cylinder can be calculated similarly, posing

$$\mathbf{f}_{xy} = \frac{\omega\mu_0}{2} Im\left[\int_{\Omega_1} (\varepsilon - \varepsilon_0)\mathbf{E}\times\mathbf{H}^* d\Omega_1\right] + Im\left[\int_{\Omega_2} (\varepsilon_c - \varepsilon_0)\mathbf{E}\times\mathbf{H}^* d\Omega_2\right]$$

In Figs. 45 is shown the total force exerted on a silica ($\varepsilon \approx 2.13$ at $f_0 = 600$ THz) cylinder with a properly designed lossless cover.

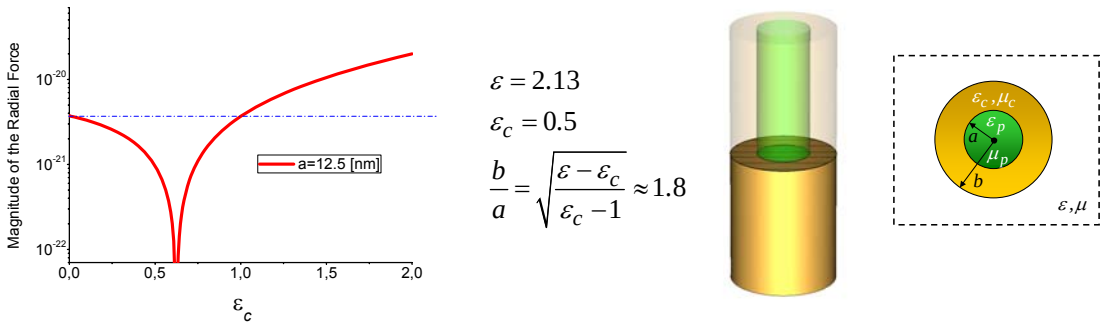

Fig. 45 Total force exerted on silica cylinder versus the cover permittivity.

It can be noticed that as the permittivity of the cover reaches the values of the surrounding space (that is $\varepsilon_c = 1$) the force exerted is equal to the one of the bare silica cylinder (Fig. 44).

4 CONCLUSIONS

We have presented the design of electromagnetic cylindrical cloaks for the TE and TM polarization at microwaves. At first, the cloak has been considered as an unbounded cylindrical shell made of an isotropic and homogenous ideal MNZ material in TE polarization or ENZ in TM polarization. Then, the effectiveness of the design has been verified through full-wave simulations considering also cylindrical objects of finite lengths. Furthermore, a proper implementation of the MNZ cloak through SRs magnetic inclusions has been proposed and verified through a set of numerical simulations. Finally, a possible layout working for both TE and TM polarizations at microwave frequencies has been suggested, by employing both the parallel plate medium layout already presented in the literature and working for the TM polarization and the SR based design for the TE polarization proposed here. We also extended the design of electromagnetic cylindrical and spherical cloaks at optical frequencies using layered structures of plasmonic and non-plasmonic materials. It is shown that a proper design of the effective layered medium, made of alternating layers of Ag and SiO_2, allows to obtain the desired ENZ behavior at the visible frequencies, allowing the actual realization of the cloaking devices for TM polarization.

5 REFERENCES

[1] Alù A., Engheta N. 2005 Phys. Rev. E 72 016623

[2] Silveirinha M. et al. 2007 Phys. Rev. E 75 036603

[3] Alù A., Engheta N. 2007 Optics Express 15 3318

[4] Alù A., Engheta N. 2007 Optics Express 15 7578

[5] Pendry J. et al. 2006 Science 312 1780

[7] Leonhardt U. 2006 Science 312 1777

[8] Cai W. et al. 2007 Nature Photonics 1 224

[9] Yan W. et al., JOSA A 25 968, 2008

[10] Gaillot D.P. et al. 2008 Optics Express 16 3986

[11] Schurig D. et al. 2006 Science 314 977

[12] Nicorovici N.A. et al. 2007 Optics Express 15 6314

[13] Alitalo P. et al. 2008 IEEE Trans. Antennas Propagat. 56 416

[14] C.A. Balanis, Anthenna Theory: Analysis and Design, Wiley, 1989

[15] C.A. Balanis, Advanced Engineering Electromagnetics, Wiley, 1982

[16] L. Tsang, J. A. Kong, Scattering of Electromagnetic Waves: Theories and Applications, Wiley, 2000

[17] H. C. Van de Hulst, Light Scattering by Small Particles, Dover, 1981

[18] Bilotti F. et al. 2007 IEEE Trans. Antennas Propagat. 55 2258

[19] Bilotti F. et al. 2007 IEEE Trans. Microwave Theory Tech. 55 2865

[20] Clemens M. et al. 2000 IEEE Trans. Magnetics 36 1448

[21] A. Nicolson, IEEE Trans. Instrum. Meas., vol. 17, pp. 395-402, Dec. 1968

[22] W. Weir, Proc. IEEE, vol. 62, pp. 33-36, Jan. 1974.

[23] B. Wood, J. B. Pendry, and D. P. Tsai, Phys. Rev. B 74, 115116, 2006

[24] C.R. Simovski, S.A. Tretyakov, "*Towards isotropic negative magnetics in the visible range,*" arXiv:0806.3512v1 [physics.optics], 21 Jun 2008

[25] Maystre D., Vincent P. "*Are optical forces derived from a scalar potential?*," *Optics Express* 15, 2007

[26] B. A. Kemp, T. M. Grzegorczyk, 2005 Optics Express 13 9280

[27] R. Loudon, S. M. Barnett, 2006 Optics Express 14 11855

[28] B. A. Kemp, T. M. Grzegorczyk, Phys. Rev. Letters 97, 133902, 2006

[29] A. R. Zakharian, M. Mansuripur, and J. V. Moloney, 2006 Optics Express 13 2321

[30] E. Grün, “Interplanetary dust and the zodiacal cloud”. Encyclopaedia of the solar system. Editors: P. Weissman, L.-A. McFadden, T. Johnson Academic Press, 1999.